Superdiffusive Heat Transport in a class of Deterministic One-Dimensional Many-Particle Lorentz gases

Pierre Collet[1]**, Jean-Pierre Eckmann**[2,3] **and Carlos Mejía-Monasterio**[4]

[1]Centre de Physique Théorique, CNRS UMR 7644, Ecole Polytechnique, F-91128 Palaiseau Cedex (France)
[2]Département de Physique Théorique, Université de Genève
[3]Section de Mathématiques, Université de Genève
[4]Istituto dei Sistemi Complessi, Consiglio Nazionale delle Ricerche, Sesto Fiorentino Italy

Abstract

We study heat transport in a one-dimensional chain of a finite number N of identical cells, coupled at its boundaries to stochastic particle reservoirs. At the center of each cell, tracer particles collide with fixed scatterers, exchanging momentum. In a recent paper, [1], a spatially continuous version of this model was derived in a scaling regime where the scattering probability of the tracers is $\gamma \sim 1/N$, corresponding to the Grad limit. A Boltzmann type equation describing the transport of heat was obtained. In this paper, we show numerically that the Boltzmann description obtained in [1] is indeed a bona fide limit of the particle model. Furthermore, we also study the heat transport of the model when the scattering probability is one, corresponding to deterministic dynamics. At a coarse grained level the model behaves as a persistent random walker with a broad waiting time distribution and strong correlations associated to the deterministic scattering. We show, that, in spite of the absence of global conserved quantities, the model leads to a superdiffusive heat transport.

1 Introduction

The rigorous description of (classical) non-equilibrium steady states (NESS) remains an elusive problem, despite some remarkable progress in the last few years, as described, *e.g.*, in [2, 3]. One of the main reasons seems to be the impossibility to guess the stationary state, which is one of the mechanisms which work in equilibrium statistical mechanics. There are therefore many studies which try to understand better what the essentials of NESS are, how different models fit together, and what are the best descriptions of NESS. Among the few works where the NESS have been obtained, we mention the harmonic chain coupled to Langevin heat baths [4] and anharmonic chains coupled to infinite (non compact) reservoirs [5, 6].

In this paper, we study heat and particle conduction in a 1-dimensional model introduced in [1], and which is a variant of a model studied in [7, 8]. We analyze several of its properties and in particular show, by numerical study, that the Boltzmann description of the model obtained in [1] is indeed a bona fide limit of the particle models studied here, but only so if the coupling, per site, is of order $\mathcal{O}(1/N)$ when the number of sites is (large) N. The model does *n*ot seem to obey the Fourier law. The reader familiar with transport problems will also notice that (due to the strictly 1-dimensional character of the model), the particle number in the NESS must be infinite. However, most of the particles will have very small kinetic energy, so that the system has very nice energy profiles, which, so to speak, are generated by those particles with energy away from 0. This is in fact reminiscent of non-normalizable measures in dynamical systems [9].

The model in question consists of a chain of identical cells, each of which contains a fixed point-like scatterer that exchanges momentum with tracer particles. Inside the system the particles move deterministically between cells, interacting with the scatterers but not among themselves. However, on their passage the particles modify the local state of the substrate, which in turns alters the evolution of the other particles. At the collisions energy is conserved. At its boundaries the chain is in contact with two stochastic particle reservoirs, characterized by a fixed temperature.

In the next section we describe in detail the model and in Sect. 3 the general properties of its non-equilibrium steady state. In Sect. 4 we study the continuous limit of our model and compare it with the theory that appeared in [1]. Finally, in Sects. 5 and 6 we discuss the energy and particle transport of the deterministic finite chain.

2   The Model

In this section, we describe the 1-dimensional particle model that we consider, and briefly review the results of [1] for the continuous model.

The model consists of N cells in a row, each cell of length λ. In the center of each cell there is a point-like scatterer which does not move but which has a "momentum" $P \in \mathbb{R}$ and a mass M. Particles move in these cells. They have mass $m \neq M$ and momentum p. The particles do not interact among themselves but they do interact with the scatterers as follows: Whenever a particle with momentum p reaches a scatterer whose momentum is P, the following happens: With probability $1 - \gamma/N$, the particle crosses to the other side of the scatterer, and continues with momentum p, while the scatterer retains its momentum P. With probability γ/N actual scattering takes place and the new momenta $\tilde{p}$ and $\tilde{P}$ are given by

$$\begin{pmatrix} \tilde{p} \\ \tilde{P} \end{pmatrix} = S \begin{pmatrix} p \\ P \end{pmatrix} ,$$

where the scattering matrix S is

$$S = \begin{pmatrix} -\sigma & 1 - \sigma \\ 1 + \sigma & \sigma \end{pmatrix} , \quad \text{and} \quad \sigma = (M - m)/(M + m) . \tag{2.1}$$

When $\gamma = N$, the particles interact with the scatterer every time they encounter one, and the model is fully deterministic, except for the nature of the baths. These rules are similar in spirit (but far more rich), to the flipping Lorentz lattice gases studied some years ago [10]. When $\gamma < N$, then the model has some randomness, since we need to decide whether scattering takes place, or the particle flies through the scatterer. Note, however, that this randomness does not change the energies of the actors in the system.

The collision rules are just those of elastic scattering, but with the scatterers not moving. The deterministic model (with $\gamma = N$) is a one dimensional generalization of the models previously studied in [7, 8, 11, 12], where the scatterers are fixed freely rotating disks. In these models, the collisions provide a local energy mixing among different degrees of freedom that leads to a local state which is well approximated by a local equilibrium state where the particles behave as a perfect gas. Close to equilibrium, Green-Kubo relations for the heat and particle fluxes are valid and the corresponding Onsager reciprocity relations are satisfied [7, 11]. Moreover, in the zero-coupling limit, where the invariant measure of the NESS is expected to be multivariate Gaussian, compact analytical expressions for the

currents and the density profiles have been obtained [8]. To the lowest order, the corrections due to a finite coupling were considered in [12]. Note that if particles and scatterers have the same mass, the model has an infinite number of conserved quantities, as their momenta are just exchanged in the collisions. Trajectories for one single particle have been considered in [13].

To force the system out of equilibrium, we couple the leftmost and rightmost cells to infinite ideal particle reservoirs. From each reservoir particles are injected into the system at a given rate ν and with momenta distributed according to

$$F(p)\,dp \;=\; \Theta(\pm p)\,(2\pi m k_{\mathrm{B}} T)^{-1/2}\,e^{-p^2/2mk_{\mathrm{B}}T}\,dp\,, \tag{2.2}$$

where T is the temperature of the reservoir, k_{B} the Boltzmann constant and the Heaviside function $\Theta(p)$ restricts the sign of the momentum according to the side from where the particles are injected ("$-$" for those entering from the right side and "$+$" for those entering from the left). Equation (2.2) implies that the particles in the vicinity of the opening between the system and the reservoir have a momentum density $f(p)$ with a non-normalizable singularity at $p = 0$. For the reservoir coupled to the leftmost ($i = 1$) cell, $f(p)$ is

$$f_{\mathrm{L}}(p)\,dp \;=\; \frac{\Theta(+p)}{(2\pi m k_{\mathrm{B}} T_{\mathrm{L}})^{1/2}}\frac{e^{-p^2/2mk_{\mathrm{B}}T_{\mathrm{L}}}}{|p|}\,dp\,, \tag{2.3}$$

and for the reservoir coupled to the rightmost ($i = N$) cell

$$f_{\mathrm{R}}(p)\,dp \;=\; \frac{\Theta(-p)}{(2\pi m k_{\mathrm{B}} T_{\mathrm{R}})^{1/2}}\frac{e^{-p^2/2mk_{\mathrm{B}}T_{\mathrm{R}}}}{|p|}\,dp\,. \tag{2.4}$$

The reader should note that the singularity of $f(p)$ is non-integrable only for one dimensional models, more precisely, for models with one dimensional dynamics. This is related to the fact that, while in any dimension, slow particles need much longer times to move across the system than fast particles, only in 1-dimensional dynamics does this imply that particles steadily accumulate near $p = 0$. In higher dimensions, $1/|p|$ is integrable near $p = 0$. Thus, the particle density diverges in the stationary state as $t \to \infty$. Due to this seemingly unphysical property, in the past, it has been argued that injecting particles with the momentum distribution (2.2) cannot be correct [14]. However, as has been shown in [1], it is the reservoir distribution $f(p)$ and not $F(p)$ that admits stationary solutions which, at the same time, preserve the distribution of the scatterers' momenta.

Furthermore, the higher momenta of p are obviously well-behaved in the limit of $t \to \infty$.

More precisely, denoting by $g(P_i)$ the distribution of the momentum of the i-th scatterer, it was shown in [1] that at equilibrium ($T_\mathrm{L} = T_\mathrm{R} = T$), both $F(p)$ and g are Gaussian and are given by

$$F(p)\, dp \;=\; (2\pi m k_\mathrm{B} T)^{-1/2} e^{-p^2/2m k_\mathrm{B} T}\, dp \;, \qquad (2.5)$$

$$g(P)\, dP \;=\; (2\pi M k_\mathrm{B} T)^{-1/2}\, e^{-P^2/2M k_\mathrm{B} T}\, dP \;. \qquad (2.6)$$

As mentioned before, because of the factor $1/|p|$ in f, the number of particles in the system is infinite at stationarity. Starting with any initial distribution, and letting the system evolve in time t, the number of particles with low momenta grows without bounds. On the other hand if one can prove that the number of particles with momentum $p > p_0$ has a limit as $t \to \infty$ then the stationary state is well defined, in spite of the divergence of the total number of particles [9]. To convince ourselves that this is indeed the case, we have measured the evolution in time of the number of particles in the system and their momentum distribution, for a chain of $N = 201$ cells at equilibrium: particles were injected from both reservoirs at the same rate $\nu = 100$ with the same temperature $T = 100$. The results are shown in Fig. 1, where the number of particles $n_t(p)$ with momentum $\approx p$ times the momentum $|p|$, is plotted for several successive times. We observe that for p larger than some $p_0(t)$, $p n_t(p)$ is stationary. This means that the total number of particles $n(t) = \int_{-\infty}^{\infty} n_t(p)\, dp$ diverges due to the slow accumulation of cold particles. Indeed, $n(t)$ diverges logarithmically with time, as can be seen in the inset of Fig. 1. In the same vein, $p_0(t)$ is seen to decrease to zero logarithmically.

In the limit of $N \to \infty$, setting $x = i/(N \cdot \lambda)$ for the position of the i-th cell, $g(P_i) \to g(P, x)$, is the probability density that the scatterer at position x has momentum P and so $\int dP\, g(P, x) = 1$, by definition. In [1] it was argued that in the continuous limit, this system can be modeled by a Boltzmann equation, whose stationary solution is described by the equations

$$p\partial_x F(p, x) = \gamma |p| \int dP \left(F(\tilde{p}, x) g(\tilde{P}, x) - F(p, x) g(P, x) \right) \;, \quad (2.7\mathrm{a})$$

$$0 = \int dp \left(F(\tilde{p}, x) g(\tilde{P}, x) - F(p, x) g(P, x) \right) \;, \qquad (2.7\mathrm{b})$$

where the quantity $F(p, x)$ is equal to $F(p, x) = |p| f(p, x)$, with $f(p, x)$ the probability density that a particle at position x has momentum p, and $\gamma \in [0, N]$ corresponds to the same quantity of the particle model, which determines the scattering
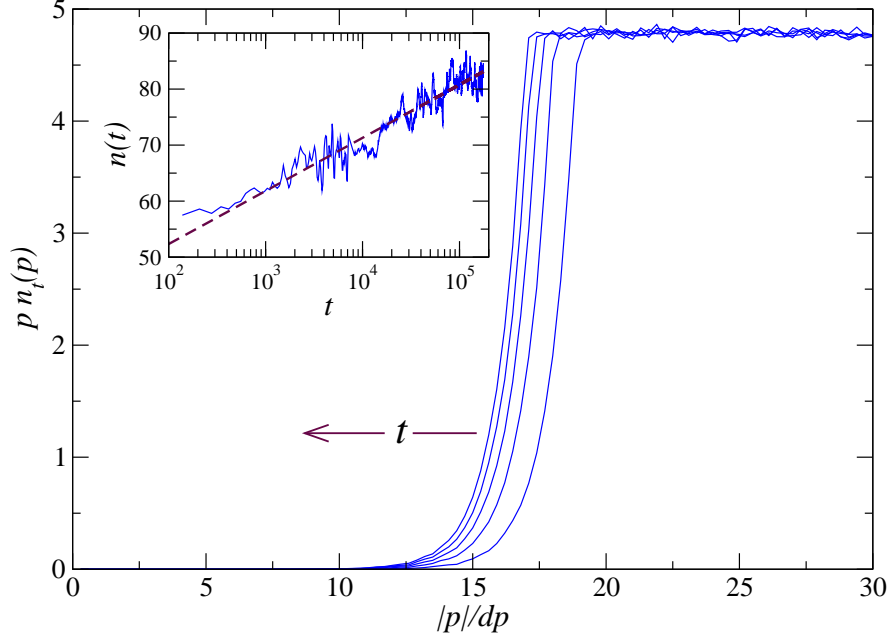
Figure 1: Number of particles $n_t(p)$ with momentum $\approx p$ times the momentum p, at $t = 200, 600, 1000, 1400$ and 1800, for a chain of $N = 201$ cells at equilibrium with $\nu_L = \nu_R = 100$ and $T_L = T_R = 100$, $\sigma = 1/2$ and $\gamma = N$. dp is the width of the bins used to compute the empirical distribution $n_t(p)$. Thus, the x-axis corresponds to the bin number. In the inset: logarithmic divergence of the total number of particles inside the system.

probability. Therefore, for $p > 0$, $F(p,x)$ is related to the rate of particles with momentum p moving from x to the right. Similarly, $F(p,x)$ is, for $p < 0$, related to the rate of particles with momentum p moving from x to the left. Note that, in contrast to $f(p)$, the function $F(p)$ is free of singularities. Therefore, in spite of the infinite number of particles in the stationary state of the scattering model, the flux $F(p,x)$ is finite and integrable, and it is for this quantity that the Boltzmann equation is formulated.

The Boltzmann equation (2.7) was derived assuming that $F(p)$ and $g(P)$ are statistically independent. Therefore, the similarity between the particle model and its Boltzmann version should be best in the case of large N and when there are many particles (with momentum $|p| > p_0 > 0$) in each cell. Moreover, in [1], it was proven that for any particle injections $f_L(p)$ and $f_R(p)$ in a certain cone in

Banach space, (2.7) has solutions when $\gamma = \mathcal{O}(1)$. Our numerical studies are, however, for parameter values well outside this cone, and still give a very good comparison between the particle model and the Boltzmann model. Furthermore, when $\gamma = \mathcal{O}(N)$, the particle model is still well defined, although different from the Boltzmann model. If $\gamma = N$ a particle will scatter whenever it meets a scatterer and will never fly to the other side of a scatterer without collision. When $\gamma \ll N$, the local state cannot correspond to a local equilibrium state. Indeed, when scattering is rare, the particles do not interact, thus leading to local states that are described by the sum of two different families of particles: those that were injected from the left, flying ballistically to the right, and those injected from the right that fly ballistically to the left [15]. However, if $\gamma = N$, then all particles scatter when they encounter a scatterer, leading to a stronger local interaction. One would expect that this strong interaction would lead to a diffusive particle behavior. However, in Sect. 5, we will show that the transport remains superdiffusive.

3 Non-equilibrium steady state

In this section we consider the model described in the previous section, coupled to reservoirs injecting particles into the chain, at different rates and at different temperatures. In the rest of the paper we will study our model for $\gamma = 1$ (corresponding to the Grad limit considered in [1]) and for $\gamma = N$ (corresponding to the deterministic particle dynamics).

Out of equilibrium, particle and energy currents appear, whose magnitudes are determined by the differences of injection rates and of temperatures. The particle injection rate is defined as

$$\nu = \int_0^\infty F(p)dp \,, \tag{3.1}$$

where $F(p)$ is the momentum distribution of the injected particles, given by (2.2). As we have discussed, the particle density in the bath is infinite. However, since the integral in (3.1) is finite, one realizes that ν takes the role of an effective particle density. Moreover, since the injected particles correspond to a perfect gas at equilibrium, one can define the chemical potential of the reservoir as

$$\mu = \mu_0 + T \log\left(\frac{\nu}{T}\right) \,, \tag{3.2}$$

with μ_0 a pure constant. The injection rate ν also trivially determines the rate at
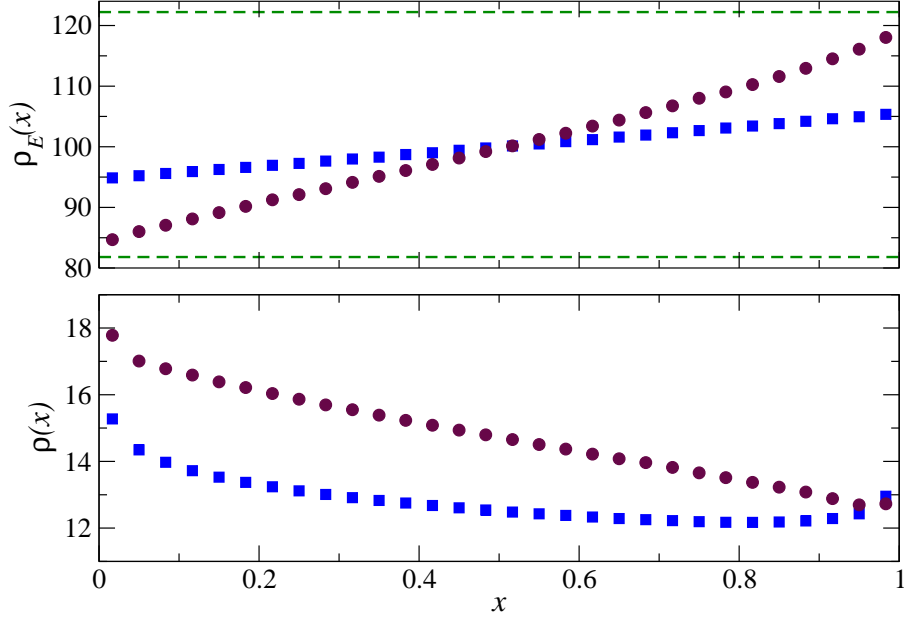
Figure 2: Profiles of the particle density (lower panel) and the kinetic energy per particle density E_K (upper panel), for a chain of $N = 30$ cells, $\sigma = 0.5$ and for $\gamma = 1$ (squares), and $\gamma = N$ (circles). Particles were injected to the chain with rates $\nu_L = 220$, $\nu_R = 180$ and temperatures $T_L = 81.818$ and $T_R = 122.222$, indicated here by the dashed line. Here, $T(x)$ is computed as the mean scatterers kinetic.

which energy is injected into the system as

$$\varepsilon = \nu k_B T \ . \tag{3.3}$$

We now proceed to study the non-equilibrium state of our model. In Fig. 2 we compare the particle density $\varrho(x)$ and the temperature profiles numerically obtained for two different values of the scattering parameter, $\gamma = 1$ and $\gamma = N$. The temperature at the i-th cell is computed as the average p^2 with respect to the particle momentum distribution function $F_i(p)$ measured at the i-th cell. This temperature coincides with the time averaged kinetic energy of the i-th scatterer, indicating a good local equilibration. All the observables were averaged for a time interval during which the total number of particles inside the channel does not change appreciably.

The temperature in the bulk of the system does not match the nominal temperatures of the reservoirs (indicated by the dashed lines in the upper panel). Moreover, we observe that the energy mismatch at the contact with the reservoirs depends on the scattering probability. For $\gamma = 1$ the temperature profile is less steep than for $\gamma = N$ as expected, since in the former case, particle-particle interaction, mediated by the scatterers, is less effective than in the latter case. As for the particle density, a smaller scattering probability leads to a less steep density profile. Moreover, the accumulation of particles at the contact with the reservoirs is more pronounced when the scattering is less frequent. This is because the scattering contributes to heat up the injected cold particles. In the limit of $N \rightarrow \infty$, the accumulation of particles at the boundaries produces singularities [14].

We also have measured the rate at which particles cross from one cell to another from left to right $\nu_{\mathrm{R}}(x)$ and from right to left $\nu_{\mathrm{L}}(x)$.

Out of equilibrium, the particles inside the cell at position x, leave the cell to the right at a different rate than the rate at which they leave the cell to the left. This is a consequence of the substrate-mediated particle-particle interaction. Calling the rate at which particles cross from one cell to another from left to right $\nu_{\mathrm{R}}(x)$ and from right to left $\nu_{\mathrm{L}}(x)$, the particle current is defined as

$$J_n(x) = \nu_{\mathrm{R}}(x) - \nu_{\mathrm{L}}(x + dx) \,. \tag{3.4}$$

Therefore, these local rates are strongly dynamically constrained, so that the stationary particle current is uniform. Indeed, we find that, in the stationary state, a uniform particle current, with extremely linear profiles for $\nu_{\mathrm{R}}(x)$ and $\nu_{\mathrm{L}}(x)$. In Sect. 5, we will see that this strong correlations determine an unexpected superdiffusive particle and energy transport.

4 Infinite volume limit: $\gamma = 1$

In this section, we compare the non-equilibrium probability distribution functions of the discrete model with those predicted by the Boltzmann equation (2.7).

We have solved numerically (2.7) by a discretization in momentum space. Fixing the spacing of the discretized momentum to Δp, the number of points we considered is the minimum necessary to keep the information from the tails of the distributions as small as $\sim 10^{-10}$. We proceed as follows: at any x, the equation (2.7b) for g only depends on $F(\cdot, x)$. We discretize (2.7b) and solve it as an eigenvalue problem (with eigenvector $g(\cdot, x)$). The only limitation is the size of the matrices one obtains in this way: Our runs were done with matrices of size
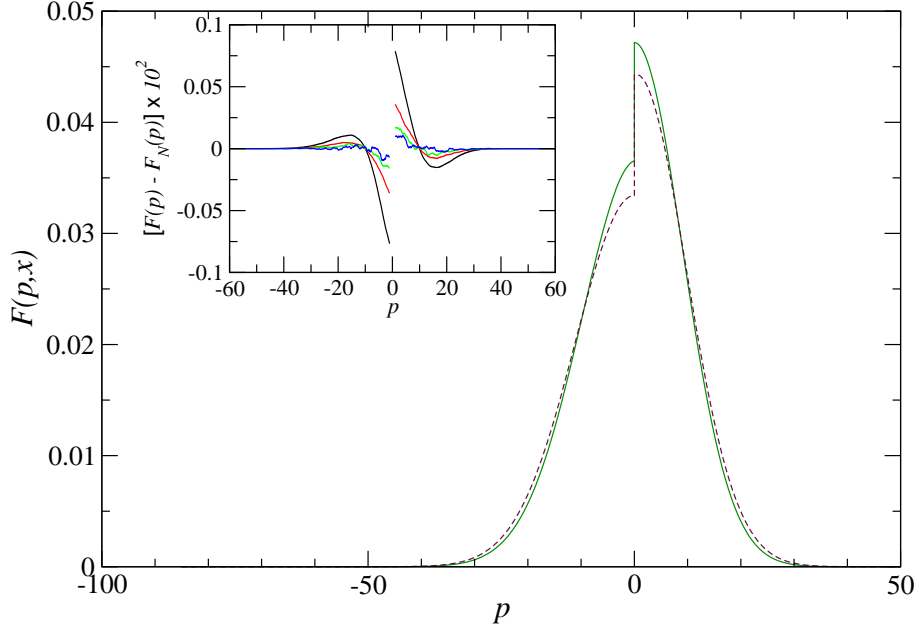
Figure 3: Momentum distribution $F(p, x)$ of the particles at the left (solid curve) and right (dashed curve) ends of the system , from the solution of the Boltzmann equation (2.7), for $\sigma = 0.5$, $\nu_L = 220$, $\nu_R = 180$, $T_L = 81.818$ and $T_R = 122.222$. In the inset the finite size deviation of $F_N(p, x)$ from the Boltzmann solution are shown for $N = 2$ (black), $N = 4$ (red), $N = 8$ (green) and $N = 16$ (blue).

~ 4200. The function g found in this way is then inserted into (2.7a). High-order integration in position space is then used to integrate (2.7a) from $x = 0$ to $x = 1$. Therefore, fixing the injection at $x = 0$ to (2.3), we use a shooting method to determine the extraction of particles at $x = 0$ in such a way that at $x = 1$ the desired injection (2.4) will result (see also [1] for more details).

In Fig. 3 we show the solution of (2.7) for $\sigma = 0.5$, $\nu_L = 220$, $\nu_R = 180$, $T_L = 81.818$ and $T_R = 122.222$, and $\gamma = 1$. The first peculiarity of the non-equilibrium distributions is the jump at $p = 0$. This is due to the very weak particle-particle interaction obtained for $\gamma = 1$. The size of the jump is partly determined by γ and, as it is clear from Eq. (3.1), partly by the difference between ν_L and ν_R. Note that, as a consequence of the temperature gradient, the positive and negative parts of the distribution are only approximately Gaussian. They are Gaussian only if $T_L = T_R$.
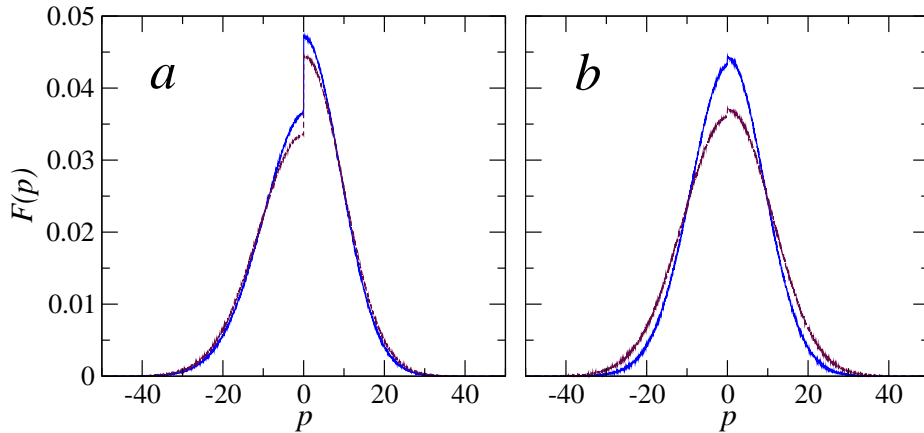
Figure 4: Momentum distribution $F_N(p, x)$ of the particles at $x = 1/N$ (solid curve) and $x = 1$ (dashed curve), for a chain of $N = 30$ cells, with $\sigma = 0.5$, for *a*) $\gamma = 1$ and *b*) $\gamma = N$. The bath's parameters are as in Fig. 3.

To study the limit $N \to \infty$, we have numerically followed the evolution of finite size N chains and measured the particle momentum distribution $F_N(p, x)$ for the same parameters as above. In the inset of Fig. 3, the deviation of $F_N(p, x)$ from the solution of the Boltzmann equation $F(p, x)$ is shown for chains from $N = 2$ to $N = 16$.

Deviations are seen over the whole domain, although they are biggest at the center of the distribution. They are not symmetric in p, which is an indication that, for a given size N, deviations may depend on the injection rates and bath's temperatures in general. Furthermore, we observe that the solution of (2.7) appears to be the asymptotic distribution, $\lim_{N \to \infty} F_N(p, x) \to F(p, x)$. In any case, the deviations from $F(p, x)$ are less than 0.1%, tending to zero very fast. For instance, for a chain of $N = 16$ the deviations are less than 0.01%.

Finally, we have also measured the distribution $F_N(p, x)$ for the deterministic finite chain ($\gamma = N$). In Fig. 4, we show $F_N(p, x)$ at $x = 1/N$ (solid curve) and $x = 1$ (dashed curve), for a chain of $N = 30$ cells and $\gamma = 1$ (panel *a*), $\gamma = N$ (panel *b*). The other parameters are reported in the caption of Fig. 3. The distributions $F_{30}(p, x)$ in Fig. 4-*a*, are on top of the solution (2.7) and, as mentioned above, the deviations from the asymptotic distribution decay very fast. For $\gamma = N$, the jump at $p = 0$ is much smaller, with the only remaining the contribution coming from the difference $|\nu_{\rm L} - \nu_{\rm R}|$ of the injection rates. As expected, the distributions

in Fig. 4-b are not Gaussian for this non-equilibrium case.

5 Energy transport

In this section we turn our attention to the heat transport of the deterministic model, *i.e.*, setting $\gamma = N$. The particles of mass m (which we call tracers) are the only energy carriers of the system. We start by analyzing their dynamics.

5.1 Microscopic evolution

We consider a finite chain of N cells with periodic boundary conditions and n particles *per cell*. A stationary state of this closed system is the equilibrium state characterized by N, n and the total energy E given by

$$E_0 = \frac{1}{2} \left(\frac{1}{m} \sum_{i=1}^{n} p_i^2 + \frac{1}{M} \sum_{i=1}^{N} P_i^2 \right) . \tag{5.1}$$

We start the evolution with the scatterers at 0 momenta. As for the open chain, the state of the system approaches equilibrium logarithmically slowly (in time). During the transient, the substrate continuously extracts energy from the gas of particles; the total energy of the scatterers grows logarithmically in time, until it saturates at sufficiently long times. All measurements are taken after the system has relaxed to the approximate equilibrium state.

Once equilibrium is reached, we focus on the evolution of a tagged particle in the bulk of the system, when N and n are sufficiently large. This is convenient, since particles interact among themselves only through their collisions with the substrate, and thus the local dynamics depends on the particle density. Here, we are interested in the high density regime, which, following the discussion about Fig. 1, is a good approximation of the stationary $n = \infty$ state.

When the particle encounters a scatterer, its velocity after collision is determined by (2.1). In fact, this scattering matrix leads to a persistent motion of the particle, namely the probability that the particle continues in the same direction in which it reached the scatterer, is larger than $1/2$. This probability, μ, can be easily computed as follows[1]: without loss of generality assume that before the collision, the particle's velocity is $v > 0$. In equilibrium, the scatterer velocity distribution function is obtained by taking $V = P/M$ in (2.6). Taking into account that after the collision the particle's velocity is $v' = -\sigma v + (1 + \sigma)V$ (see (2.1)), the

---

[1]To analyze the dependence of μ on the masses, it is convenient to work with the velocities instead of the momenta.

probability that after the collision the particle has a velocity $v' > 0$ can be written as[2]

$$\mu(\sigma) \equiv P(v' > 0 | v > 0) = \frac{(mM)^{1/2}}{2\pi k_{\mathrm{B}} T} \int_0^\infty dv \; e^{-\frac{mv^2}{2k_{\mathrm{B}}T}} \int_{\frac{\sigma}{1+\sigma}v}^\infty dV e^{-\frac{MV^2}{2k_{\mathrm{B}}T}} \; , \quad (5.2)$$

that can be integrated to yield

$$\mu(\sigma) = \frac{1}{2} - \left(\frac{m}{2\pi k_{\mathrm{B}} T} \right)^{1/2} \int_0^\infty dv \; \mathrm{erf}\left(\frac{(M-m)v}{(8 M k_{\mathrm{B}} T)^{1/2}} \right) e^{-\frac{mv^2}{2k_{\mathrm{B}}T}} \; , \quad (5.3)$$

where $\mathrm{erf}(\cdot)$ is the error function. The limit values of μ can be easily read from (5.3): for $\sigma = -1$, namely $M = 0$, the error function is $\mathrm{erf}(-\infty) = -1$ and $\mu = 1$. In the opposite case, when $\sigma = 1$ ($M = \infty$), $\mu = 0$. Finally, for $\sigma = 0$, namely $M = m$, $\mathrm{erf}(0) = 0$ and $\mu = 1/2$. With the exception of $\sigma = 0$, the dynamics of the particles is persistent. In Fig. 5, the probability $\mu(\sigma)$, computed from the statistics of the collisions of the tagged particle is shown.

At a coarse grained description, the dynamics of the particles can be seen as a persistent random walk with waiting time τ corresponding to the collision times, that are determined by the particle's velocity. We have measured the distribution of the waiting time $\Psi(\tau)$ of the tagged particle for different values of σ. In Fig. 6 we show $\Psi(\tau)$ for $\sigma = 0$ and $\sigma = 0.5$. As a consequence of the single particle's velocity distribution, $\Psi(\tau)$ turns out to be a broad distribution $\Psi(\tau) \simeq \tau^{-(1+s)}$, with $s \simeq 1$ for $\sigma = 0.5$ and $s \simeq 2$ for $\sigma = 0$. Therefore, our persistent walker seemingly performs a Levy walk. The power -2 for $\sigma \neq 0$ can be derived (approximately) from a multiple integral as in (5.3).

In the continuous limit, a persistent random walker yields to a particle's density whose evolution is described by the telegraph equation [16]. Noting that asymptotically the telegraph equation yields to a diffusive evolution and that the Levy walk for $1 < s < 2$ does only induce anomalous corrections to the normal long-time behavior [17], one would expect that the microscopic particle's dynamics yields diffusive transport. However, this is not the case. In Fig. 7 we show the evolution of the dispersion of the position of a tagged particle $\langle x^2(t) \rangle$ for $\sigma = 0.5$, averaged over an ensemble of initial conditions. Asymptotically, $\langle x^2(t) \rangle \sim t^\alpha$, with $\alpha \lesssim 2$. In fact, we have found that the asymptotic scaling of $\langle x^2(t) \rangle$ depends on the mass ratio parameter σ (see inset of Fig. 7). For $\sigma = 0$ the particle's motion

---

[2]There is no factor $1/|v|$ here, because we must consider the probability of a particle with velocity in $[v, v + dv]$ hitting a scatterer within a given time.
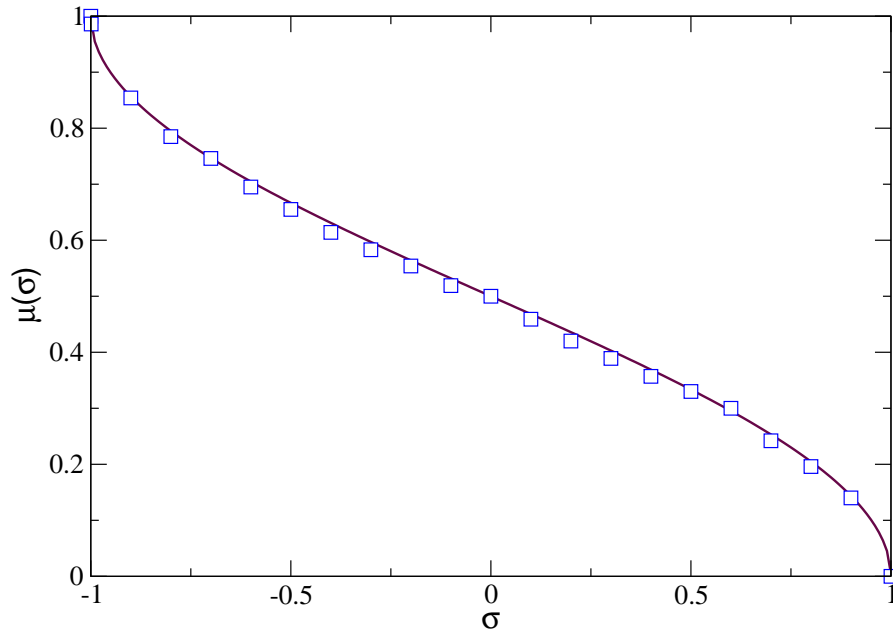
Figure 5: Persistent probability μ as a function of the mass ratio parameter σ, averaged over the evolution of a tagged particle in a chain of $N = 11$, $n = 20$ and $T = 500$.

is ballistic, while for $\sigma \neq 0$, the motion is superdiffusive. The observed anomalous behavior proves that in one dimension, the effect of the dynamical memory of the deterministic model is much stronger than in higher dimensions[3]. Since the particles are the energy carriers one expects that the energy transport will be anomalous as well. We study this in the next section.

6 Heat conductivity

We turn our attention to the energy transport of our model. Considering the open system coupled at its boundaries to two particle reservoirs, we have computed the dependence of the heat conductivity κ on the size of the system N, for fixed nominal values of the injections and temperatures of the particle reservoirs. We

---

[3]As a note aside, if the direction of the particle after the collision if chosen randomly so that the effects of the dynamical memory can be neglected, then the diffusive transport is recovered.
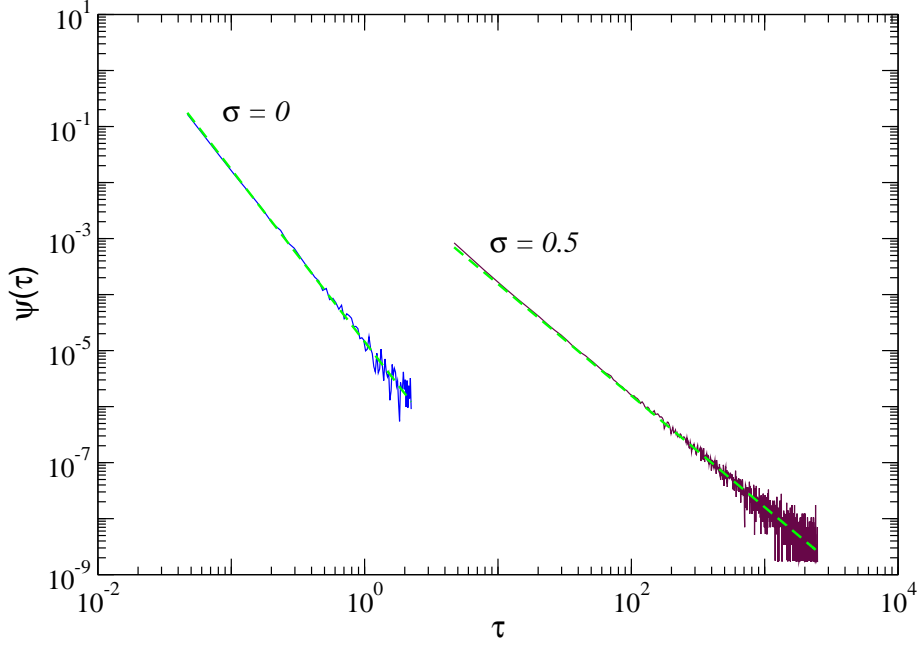
Figure 6: Distribution function of the collision times $\Psi(\tau)$, for $\sigma = 0$ and $\sigma = 0.5$. The dashed lines correspond to fit to a power law. We obtain, in within numerical accuracy, $\Psi(\tau) \sim \tau^{-3}$ for $\sigma = 0$ and $\Psi(\tau) \sim \tau^{-2}$ for $\sigma = 0.5$.

define the heat conductivity as

$$\kappa = \frac{J_U}{T_N - T_1} \ ,$$

where J_U is the measured energy current and T_1 (resp. T_N) is the temperature measured in the leftmost (resp. rightmost) cell that, as we have seen, in general does not coincide with the temperatures of the reservoirs. (The length of the system is 1 since we space the scatterers by $\lambda = 1/N$.) The results of simulations are shown in Fig. 8 for $\gamma = 1$ (squares) and $\gamma = N$ (circles). When the scattering is rare ($\gamma = 1$), we obtain $\kappa \sim N$. This can be understood from the fact that particles move ballistically, interacting with the lattice very rarely.

Surprisingly, the energy transport in the deterministic model ($\gamma = N$) is anomalous, with a heat conductivity that diverges as $\kappa \sim N^{1/3}$. It is interesting to note that usually anomalous heat conduction is related to the existence of additional global conserved quantities [3]. However, for $\sigma \neq 0$ the bulk dynamics
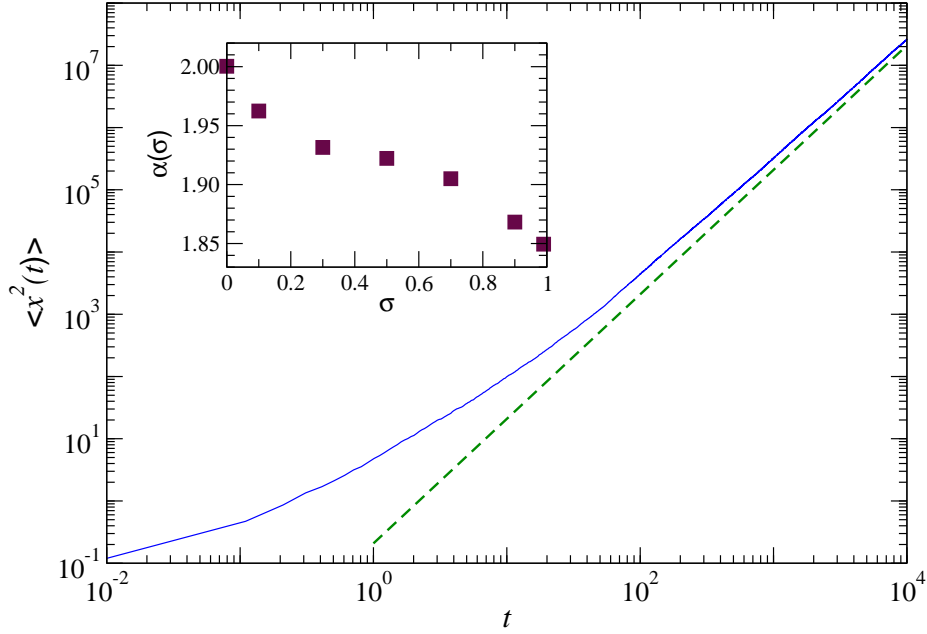
Figure 7: Time dependence of the variance of the position of the tagged particle $\langle x^2(t) \rangle$, for $N = 11$, $n = 20$ and temperature $T = 500$ (solid curve), when $\sigma = 1$. The dashed line corresponds to a scaling $\sim t^2$. In the inset, asymptotic power scaling $\langle x^2(t) \rangle \sim t^{\alpha}$, as a function of the mass ratio parameter σ.

of our model only conserves energy. As far as we know, this is the first example of a mechanical model that, not having additional integrals of motion, shows anomalous heat conduction.

6.1   Return to equilibrium

In order to shed more light on the anomalous heat transport we studied the system's equilibrium response to a finite energy perturbation. Suppose that at a certain initial time, $t = 0$, the equilibrium state of the system is perturbed by an additional amount of energy ΔE that is distributed among all the degrees of freedom in a finite region of volume V, around the position x. By measuring the evolution of the energy field, one can estimate how heat propagates through the system.

Considering the closed system as in Sect. 5.1 we proceed as follows: at time $t = 0$ we perturb the state S^0 of the system to $\tilde{S}$, as follows: the energies of the
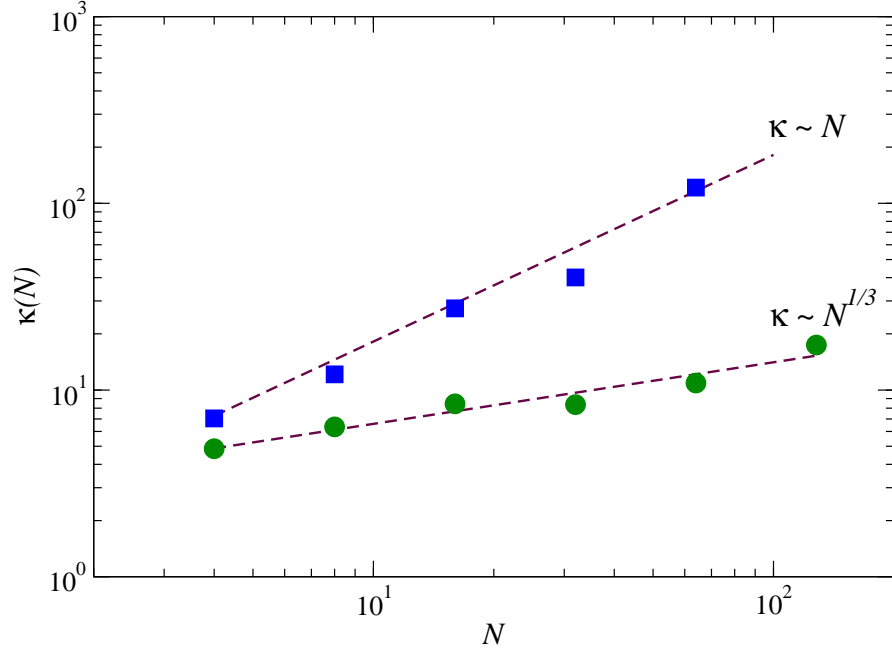
Figure 8: Heat conductivity κ, as a function of the number of cells N, for two values of γ: 1 (squares) and N (circles). The rest of the system's parameters are as in Fig. 3. For $\gamma = N$, κ diverges as $\sim N^{1/3}$, while for $\gamma = 1$, κ diverges as $\sim N$. These power laws are indicated by the dashed lines.

particles and scatterers contained in the $\mathcal{N}$ central cells are changed so that the total energy inside these cells is E_{pert}. After this, we let the central subsystem relax. To obtain the evolution of the energy perturbation $\Delta E(x, t)$, we have followed two trajectories of the system: the unperturbed one, with initial state S^0 and the perturbed one, with initial state $\tilde{S}$. Then, the energy difference at time t and position x is

$$\Delta E(x = i\lambda, t) = \langle \tilde{E}_i(t) - E_i^0(t) \rangle , \tag{6.1}$$

where $\tilde{E}_i(t)$ is the energy contained in the ith cell at time t of the perturbed trajectory and respectively for $E_i^0(t)$, and $\langle \cdot \rangle$ denotes the average over an ensemble of different initial realizations.

When dynamical correlations are not too strong, one expects that after a sufficiently long time the perturbation $\Delta E(x, t)$ scales (with x measured from the
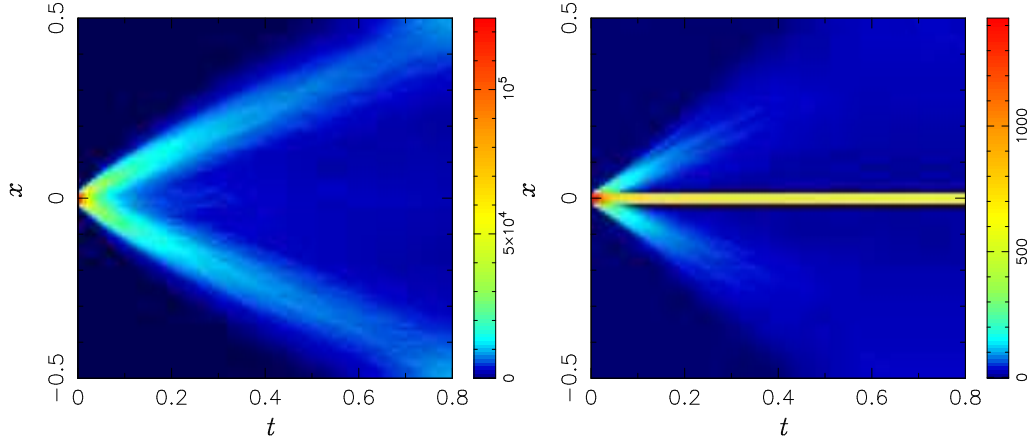
Figure 9: Evolution of the energy difference $\Delta E(x, t)$ for a chain of $N = 101$, $n = 50$ and $\sigma = 0.5$, and for $\gamma = N$ (left panel) and $\gamma = 1$ (right panel). The initial energy per degree of freedom was $\varepsilon^0 = 5000$ and $\tilde{\varepsilon} = 50000$.

initially perturbed cells) as

$$\Delta E(x, t) = \frac{1}{t^\xi} \Delta E\left(\frac{x}{t^\xi}, t\right) , \tag{6.2}$$

where the power ξ is related to the scaling of the heat conductivity with the size of the system L as [18]:

$$\kappa = N^{2-1/\xi} . \tag{6.3}$$

In particular, $\xi = 1/2$ corresponds to normal diffusion, while $\xi = 1$ corresponds to ballistic motion.

In Fig. 9 we show the evolution of the energy difference $\Delta E(x, t)$ for the deterministic chain $\gamma = N$ (left panel) and compare it with the stochastic chain with $\gamma = 1$ (right panel). We observe that for $\gamma = N$, the initial excess of energy at the central cell decays very rapidly. Practically none of the initial energy remains in the central cell. The perturbation moves symmetrically to the ends of the chain, carried by two seemingly independent families of particles, those with positive velocity and those with negative velocity. Actually, it is the fast decay of the energy at the center that marks the existence of very strong dynamical correlations. A similar observation has been made recently in a random walk with memory in the waiting times of successive steps [19]. For $\gamma = 1$, we also observe an initial fast decrease of the energy perturbation. The evolution of the peaks with
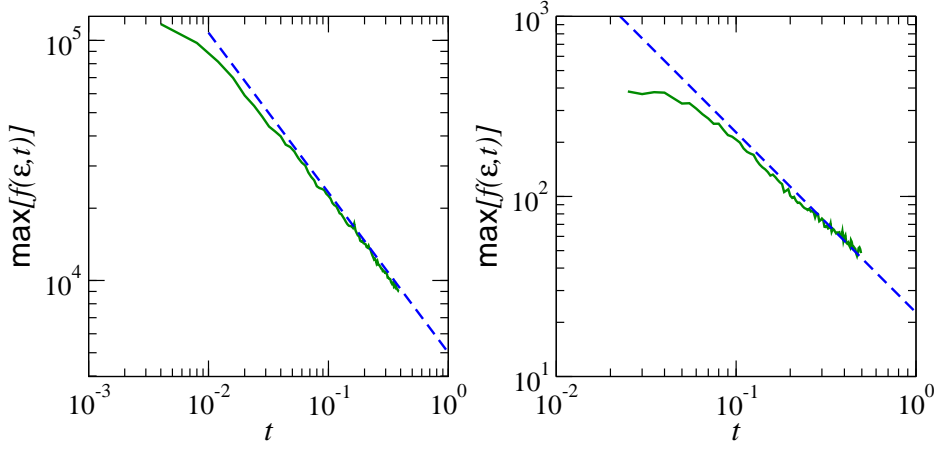
Figure 10: Damping of the maximum value of $\Delta E(x,t)$ as a function of time, for the same simulation as in Fig. 9, for $\gamma = N$ (left panel) and $\gamma = 1$ (right panel). The dashed curves corresponds to the power law $t^{-2/3}$ for $\gamma = N$ and to t^{-1} for $\gamma = 1$.

positive and negative velocity seems to move ballistically. On the other hand, when $\gamma = N$, the group velocity of the outgoing peaks depends weakly on time, probably reaching a final constant velocity at much longer times.

The scalings (6.2) and (6.3) are valid for the decaying of the initial perturbation, namely they are valid if measured from the decay of the central peak. Nevertheless, we find that in our case, similar scalings are possible for the outgoing peaks. Assuming that the excess of energy is transported across the system as a density packet, whose area is preserved on average, we show in Fig. 10 the damping of the amplitude of the moving peak as a function of time. For $\gamma = N$ (left panel), the amplitude of the peak decays as $t^{-2/3}$, corresponding to a heat conductivity that scales as $\kappa \approx N^{1/2}$. Note, however, that within numerical accuracy, the decay could also be consistent with $\kappa \approx N^{1/3}$ as it is found at the beginning of this section. In fact, from a fit to a power law of the amplitude decay we have obtained scalings for the amplitude decay between 0.62 to 0.66. In any case, the spreading of the outgoing peak reflects, locally, the anomalous character of the heat transport. On the other hand, the amplitude decay for $\gamma = 1$ (right panel) is consistent with t^{-1}, corresponding to a heat conductivity that grows linearly with N, in full agreement with the observations at the beginning of this section.

Acknowledgements

References

[1] P Collet and J-P Eckmann. A model of heat conduction. *arXiv:0804.3025*, 0804:3025, 2008.

[2] F Bonetto, J L Lebowitz, and L Rey-Bellet. *Mathematical Physics 2000*. Imperial College, London, 2000.

[3] S Lepri, R Livi, and A Politi. Thermal conduction in classical low-dimensional lattices. *Phys. Rep.*, 377:1, 2003.

[4] Z Rieder, J L Lebowitz, and E Lieb. Properties of a harmonic crystal in a stationary nonequilibrium state. *J. Math. Phys.*, 8:1073, 1967.

[5] J-P Eckmann, C A Pillet, and L Rey-Bellet. Non-equilibrium statistical mechanics of anharmonic chains coupled to two heat baths at different temperatures. *Commun. Math. Phys.*, 201:657, 1999.

[6] Jean Bricmont and Antti Kupiainen. Towards a derivation of Fourier's law for coupled anharmonic oscillators. *Comm. Math. Phys.*, 274(3):555–626, 2007.

[7] C Mejia-Monasterio, H Larralde, and F Leyvraz. Coupled normal heat and matter transport in a simple model system. *Phys. Rev. Lett.*, 86:5417, 2001.

[8] J-P Eckmann and L-S Young. Nonequilibrium energy profiles for a class of 1-d models. *Commun. Math. Phys.*, 262:237, 2006.

[9] P Collet and P Ferrero. Some limit ratio theorem related to a real endomorphism in case of a neutral fixed point. *Ann. Inst. Henri Poincaré*, 52:283, 1990.

[10] P Grosfils, J P Boon, E G D Cohen, and L A Bunimovich. Propagation and organization in lattice random media. *J. Stat. Phys.*, 97:575–608, 1999.

[11] H Larralde, F Leyvraz, and C Mejia-Monasterio. Transport properties of a modified Lorentz gas. *J. Stat. Phys.*, 113:197, 2003.

[12] J-P Eckmann, C Mejia-Monasterio, and E Zabey. Memory effects in nonequilibrium transport for deterministic Hamiltonian systems. *J. Stat. Phys.*, 123:1339, 2006.

[13] L A Bunimovich and M A Khlabystova. One-dimensional Lorentz gas with rotating scatterers: exact solutions. *J. Stat. Phys.*, 112:1207, 2003.

[14] R Tehver, F Toigo, J Koplik, and J R Banavar. Thermal walls in computer simulations. *Phys. Rev. E*, 57:R17, 1998.

[15] A Dhar and D Dhar. Absence of local thermal equilibrium in two models of heat conduction. *Phys. Rev. Lett.*, 82:480, 1999.

[16] G H Weiss. Some applications of persistent random walks and the telegrapher's equation. *Physica A*, 311:381, 2002.

[17] J-P Bouchaud and A Georges. Anomalous diffusion in disordered media: statistical mechanisms, models and physical applications. *Phys. Rep.*, 195:127, 1990.

[18] S Denisov, J Klafter, and M Urbakh. Dynamical heat channels. *Phys. Rev. Lett.*, 91:194301, 2003.

[19] V Y Zaburdaev. Random walk model with waiting times depending on the preceding jump length. *J. Stat. Phys.*, 123:871, 2006.